Impact of Organometallic Intermediates on Copper-Catalyzed Atom Transfer Radical Polymerization

Marco Fantin, Francesca Lorandi, Thomas Ribelli, Grzegorz Szczepaniak, Alan Enciso, Christophe Fliedel, Lucas Thevenin, Abdirisak Isse, Rinaldo Poli, Krzysztof Matyjaszewski

▶ **To cite this version:**

Marco Fantin, Francesca Lorandi, Thomas Ribelli, Grzegorz Szczepaniak, Alan Enciso, et al.. Impact of Organometallic Intermediates on Copper-Catalyzed Atom Transfer Radical Polymerization. Macromolecules, 2019, 52 (11), pp.4079-4090. 10.1021/acs.macromol.9b00870 . hal-02333008

HAL Id: hal-02333008
https://hal.science/hal-02333008

Submitted on 30 Oct 2020

HAL is a multi-disciplinary open access archive for the deposit and dissemination of scientific research documents, whether they are published or not. The documents may come from teaching and research institutions in France or abroad, or from public or private research centers.

L'archive ouverte pluridisciplinaire **HAL**, est destinée au dépôt et à la diffusion de documents scientifiques de niveau recherche, publiés ou non, émanant des établissements d'enseignement et de recherche français ou étrangers, des laboratoires publics ou privés.

The Impact of Organometallic Intermediates on Copper-Catalyzed Atom Transfer Radical Polymerization

Marco Fantin,[†,‡] Francesca Lorandi,[†,‡] Thomas G. Ribelli,[†] Grzegorz Szczepaniak,[†] Alan E. Enciso,[†,§] Christophe Fliedel,[I] Lucas Thevenin,[I] Abdirisak A. Isse,[⊥] Rinaldo Poli,[I#] Krzysztof Matyjaszewski[*†]

[†]Department of Chemistry, Carnegie Mellon University, 4400 Fifth Avenue, Pittsburgh, Pennsylvania 15213, United States

[§]Department of Chemistry, Northwestern University 2145 Sheridan Road, Evanston, IL 60208 (USA)

[I]CNRS, LCC (Laboratoire de Chimie de Coordination), Université de Toulouse, UPS, INPT, 205 Route de Narbonne, F-31077 Toulouse Cedex 4, France

[⊥]Department of Chemical Sciences, University of Padova, via Marzolo 1, 35131 Padova, Italy

[#]Institut Universitaire de France, 1 Rue Descartes, 75231 Paris Cedex 05, France

Abstract

In atom transfer radical polymerization (ATRP), radicals ($R^{\bullet}$) can react with Cu^{I}/L catalysts forming organometallic complexes, R-Cu^{II}/L (L = N-based ligand). R-Cu^{II}/L favors additional catalyzed radical termination (CRT) pathways, which should be understood and harnessed to tune the polymerization outcome. Therefore, the preparation of precise polymer architectures by ATRP depends on the stability and on the role of R-Cu^{II}/L intermediates. Herein, spectroscopic and electrochemical techniques were used to quantify the thermodynamic and kinetic parameters of the interactions between radicals and Cu catalysts. The effects of radical structure, catalyst structure, and solvent nature were investigated. The stability of R-Cu^{II}/L depends on the radical stabilizing group in the following order: cyano > ester > phenyl. Primary radicals form the most stable R-Cu^{II}/L species. Overall, the stability of R-Cu^{II}/L does not significantly depend on the electronic properties of the ligand, contrary to the ATRP activity. Under typical ATRP conditions, the R-Cu^{II}/L build-up and the CRT contribution may be suppressed by using more ATRP-active catalysts or solvents that promote a higher ATRP activity.

Introduction

The fabrication of better and smarter "soft" materials relies on the ability to tailor the architecture and composition of polymers, which can be achieved by living or controlled polymerization techniques. For monomers that can polymerize radically, reversible-deactivation radical polymerization (RDRP) methods are commonly used. Two of these methods, atom transfer radical polymerization (ATRP)[1] and organometallic mediated radical polymerization (OMRP),[2] make use of transition metal complexes, although with different mechanisms.

In ATRP, a metal complex catalytically and intermittently removes a halogen atom from the polymer chain end. This results in the periodic formation of active species ($R^{\bullet}$, radicals) from dormant ones (RX, halogen-capped chains), thus allowing for polymerization control.[3, 4] The most commonly used metal in ATRP is copper, ligated by N-based ligands (L) to form a complex that alternates between Cu^{I} (activator) and Cu^{II} (deactivator) oxidation states. The Cu^{I}/L activator generates radicals (with rate coefficient $k_{a,ATRP}$, Scheme 1, red box) that adds a few monomer units before being deactivated by the X-Cu^{II}/L complex (with rate coefficient $k_{d,ATRP}$). The ATRP equilibrium constant, $K_{ATRP} = k_{a,ATRP}/ k_{d,ATRP}$, is usually << 1 to maintain a low and steady radical concentration. Originally, ATRP required relatively high loadings of a copper complex in equimolar amounts to RX.[5] More recent ATRP techniques enable the use of a catalytic amount of copper, with the concurrent regeneration of the Cu^{I}/L activator.[6-8]

In OMRP, the radical chain end binds directly to the metal center to alternate between active (radical) and dormant (metal-capped) species.[9] Therefore, OMRP requires stoichiometric amounts of the metal complex relative to the polymer chains, rather than catalytic amounts. Cobalt is the most common metal in OMRP.[10, 11] OMRP complexes add to polymer chains deactivating them with rate coefficient $k_{d,OMRP}$. The dissociation of the complex (i.e. OMRP activation) has rate constant $k_{a,OMRP}$ (Scheme 1, green box, for the case of copper complexes). Therefore, the OMRP equilibrium constant, $K_{OMRP} = k_{a,OMRP}/ k_{d,OMRP}$, should also be << 1 to keep a sufficiently low radical concentration.

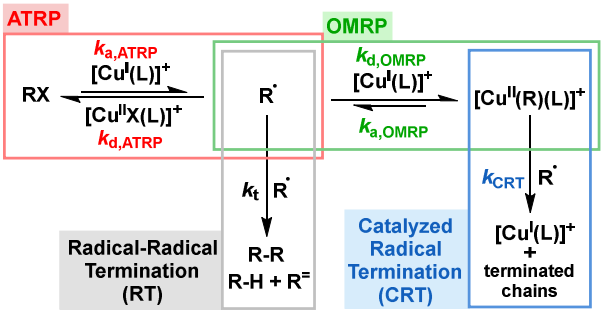

Scheme 1. ATRP equilibrium of radical activation/deactivation (red box); bimolecular radical termination, (RT, gray box); formation and dissociation of organometallic species in OMRP (green box); catalyzed radical termination (CRT, blue box).

The ATRP and OMRP polymerization mechanisms are not always independent but can instead coexist as indicated in Scheme 1.[12-14] It has been recently recognized that Cu^{I} ATRP catalysts not only activate RX, but can also directly trap radicals, forming organometallic intermediates R-Cu^{II}/L (Scheme 1, green box).[1] In typical ATRP polymerizations, R-Cu^{II}/L species are low-concentration intermediates that have been elusive and difficult to detect. There has been evidence, however, of their influence on polymerizations since early reports by Matyjaszewski *et al.*:[15] for methyl acrylate (MA), the rate of polymerization was decreased in the presence of Cu^{I}OTf/L complexes (OTf = trifluoromethanesulfonate).

Buback *et al.* first proposed the use of EPR spectroscopy to observe the formation of R-Cu^{II}/L.[16] In the presence of Cu^{I}/L complexes (L = tris(2-pyridylmethyl)amine, TPMA), the rate of termination of butyl acrylate radicals was faster than predicted on the basis of radical-radical termination, and a new distinct EPR transient was detected. A new interesting way to generate $[Cu^{II}(R)(L)]^{+}$ was recently introduced by Bernhardt *et al.*, making use of an electrochemical ATRP activation step to generate radicals.[17, 18] In cyclic voltammetry (CV), $[Cu^{II}Br(L)]^{+}$ complexes were reduced *in situ* to $[Cu^{I}Br(L)]$. This catalyst dissociated Br^{-} yielding $[Cu^{I}(L)]^{+}$, which reacted with RBr generating radicals by ATRP activation. Moreover, the same $[Cu^{I}(L)]^{+}$ complex reacted with radicals in the OMRP process to form $[Cu^{II}(R)(L)]^{+}$. These reactions had a considerable effect on the shape of the CV traces. A fitting procedure was used to extract thermodynamic and kinetic parameters on the formation of $[Cu^{II}(R)(L)]^{+}$.

The presence of $[Cu^{II}(R)(L)]^{+}$ species is linked to the phenomenon of catalyzed radical termination (CRT) promoted by organocopper(II) species.[19, 20] Under conditions where excess

radicals with respect to $[Cu^{I}(L)]^{+}$ were produced, the radical termination rate significantly increased. This additional mode of termination is the dominant one for the ATRP of methyl acrylate in CH_3CN, being up to 40 times faster than the bimolecular radical termination (RT) by radical-radical reactions.[19] Different pathways are possible for this catalyzed process, leading to either radical-radical coupling or disproportionation products, but all appear to require the formation of a R-Cu^{II}/L intermediate (Scheme 1, blue box). The possible involvement of a hydride intermediate in the mechanism was excluded by computational studies.[18, 21]

Despite the significant role of organometallic intermediates in ATRP, their contributions during polymerizations have not yet been quantified nor the intimate mechanism of the CRT process has been elucidated.[20, 22, 23] This is in part linked to the difficulty of obtaining reliable information on the fast reactions involved in ATRP and OMRP equilibria. The deactivation of radicals by $[Cu^{II}Br(L)]^{+}$ and their trapping by $[Cu^{I}(L)]^{+}$ are very fast reactions that approach the diffusion limit for a second-order process.[17] This explains why so few experimental data are available, which makes it difficult to predict and understand the interplay between ATRP, OMRP, and CRT. Fortunately, it has been recently shown that electrochemical methods can be used to study quantitatively the reactions in Scheme 1, for both the ATRP[24-30] and OMRP processes.[17,18]

In this contribution, we set forth to determine the stability and rate of formation of a variety of Cu-organometallic complexes $[Cu^{II}(R)(L)]^{+}$ with the ligands and initiators shown in Scheme 2: L = TPMA or substituted derivatives and R = $CH_{2-n}Me_nX$ where X is either CN (n = 0, 1), COOR' (R' = Et for n = 0, 2; R' = Me for n = 1) or Ph (n = 0, 1). The organometallic intermediates were generated by direct one-electron oxidative addition of RBr to $[Cu^{I}(L)]^{+}$, following the reaction by stopped-flow techniques (for fast reactions such as the ATRP activation step or the formation of $[Cu^{II}(R)(L)]^{+}$) or traditional UV-Vis spectroscopy (for slower reactions such as the dissociation of $[Cu^{II}(R)(L)]^{+}$). The spectroscopic data were supplemented by a modification of the electrochemical approach introduced by Bernhardt et *al.*[17, 18] The following three modifications were introduced: i) we accounted for CRT, which we found to have an impact in the case of acrylate radicals, ii) we used spectroscopic data to determine the rate constant of dissociation of the most stable $[Cu^{II}(R)(L)]^{+}$ complexes (which have a longer lifetime than the timescale of a typical CV measurement), iii) we subtracted the background current from the CV measurements—a common practice in electrochemical simulations as well as a solution that allowed for an improvement of the quality of the simulated data. Overall, the combination of spectroscopic and

electrochemical data allowed us to evaluate the importance of $[Cu^{II}(R)(L)]^+$ species in the polymerization of the most commonly employed monomers, including acrylates, methacrylates, acrylonitrile, and styrene. The effect of catalyst activity was also analyzed, by using three different amine ligands that gave ATRP catalysts in an activity range of 5 orders of magnitude. Furthermore, four of the most commonly used polar solvents in ATRP were considered: DMF, acetonitrile, DMSO, and water.

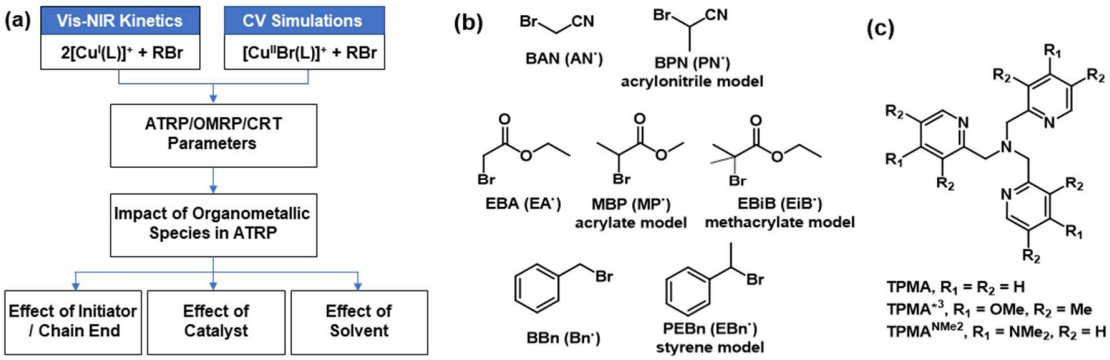

Scheme 2. (a) Workflow of determining the role of organometallic species in ATRP; (b) structures of investigated initiators (the terms in parentheses indicate the corresponding radicals after bromine transfer) and (c) structures of the investigated copper ligands.

Finally, introducing catalyzed radical termination in our model allowed us to examine the role of $[Cu^{II}(R)(L)]^+$ in promoting radical termination. Copper-promoted radical termination was found to be negligible (or very slow) for nitrile-stabilized radicals (i.e. the propagating species of acrylonitrile) and for phenyl-stabilized ones (i.e. the propagating species of styrene), but more pronounced for ester-stabilized radicals (i.e. acrylates). In particular, the initiator methyl 2-bromopropionate (MBP, acrylate mimic) appeared to undergo formation of $[Cu^{II}(R)(L)]^+$, followed by Cu-mediated radical termination.

Overall, the analysis of these results gave some insight into questions such as: Can we control polymer growth with Cu-based OMRP? What is the impact of OMRP and CRT for different monomers?

Results and discussion

Tracking $[Cu^{II}(R)(L)]^+$ under Stopped-Flow Conditions. Complexes $[Cu^{II}(R)(L)]^+$ (L = TPMA) were generated in bulk and observed spectroscopically by mixing $[Cu^{I}(TPMA)]^+TfO^-$ with the

highly active bromoacetonitrile (BAN) or 2-bromopropionitrile (BPN) initiators in a 2:1 ratio. The reactions occurring in these systems are described in Scheme 3. The reaction cycle starts from the ATRP-active catalyst $[Cu^{I}(TPMA)]^{+}$ because TfO^{-} is a non-coordinating anion. ATRP activation ($k_{a,ATRP}$) generates $R^{\bullet}$, which can either be deactivated in the reverse reaction by $[Cu^{II}Br(L)]^{+}$ ($k_{d,ATRP}$), terminate with a second $R^{\bullet}$ (k_t), or be trapped by $[Cu^{I}(L)]^{+}$ to form $[Cu^{II}(R)(L)]^{+}$ ($k_{d,OMRP}$). It should be noted that the halogen affinity (i.e. halidophilicity) of both Cu^{II} and Cu^{I} species strongly influences the availability of ATRP deactivator and activator, respectively, and therefore it has to be considered in the mechanism. A molar Cu^{I}/RBr ratio of 2:1 ensured the presence of sufficient $[Cu^{I}(L)]^{+}$ complex to trap the radicals generated in the ATRP activation ($AN^{\bullet}$ or $PN^{\bullet}$). The formation of $[Cu^{II}Br(L)]^{+}$ and $[Cu^{II}(R)(L)]^{+}$ was followed spectroscopically, adopting a stopped-flow technique[31] to follow the rapid sequence of reactions in Scheme 3. Figure 1a shows the evolution of the visible spectrum in the first 2.4 seconds after mixing the $[Cu^{I}(TPMA)]^{+}$ and BAN solutions.

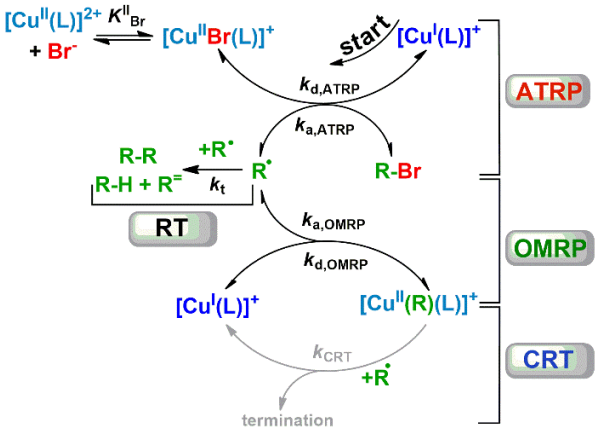

Scheme 3. Mechanism of ATRP, OMRP, RT, and, when relevant, CRT

The evolution of the Cu^{II} species concentration could be obtained from Figure 1a. Both Cu^{I} and Cu^{II} species absorb at wavelengths < 550 nm; therefore, the lower wavelength part of the spectra was disregarded. The evolution of the band with maximum at 600 nm corresponds to the formation of $[Cu^{II}(CH_2CN)(TPMA)]^{+}$, while the signal at 725 nm has contributions from both the absorbance of $[Cu^{II}(CH_2CN)(TPMA)]^{+}$ and $[Cu^{II}Br(TPMA)]^{+}$.[17] Deconvolution of the spectra based on literature data[17] (as described in section S1.6 of the Supporting Information) allowed us to track the concentration of both $[Cu^{II}(CH_2CN)(TPMA)]^{+}$ and $[Cu^{II}Br(TPMA)]^{+}$ species in time,

which is plotted in Figure 1b. The two complexes were generated at the same rate, indicating that the ATRP activation is the rate determining step of the process and that all the generated radicals were quickly trapped by $[Cu^{I}(TPMA)]^{+}$ with no significant radical loss by termination.

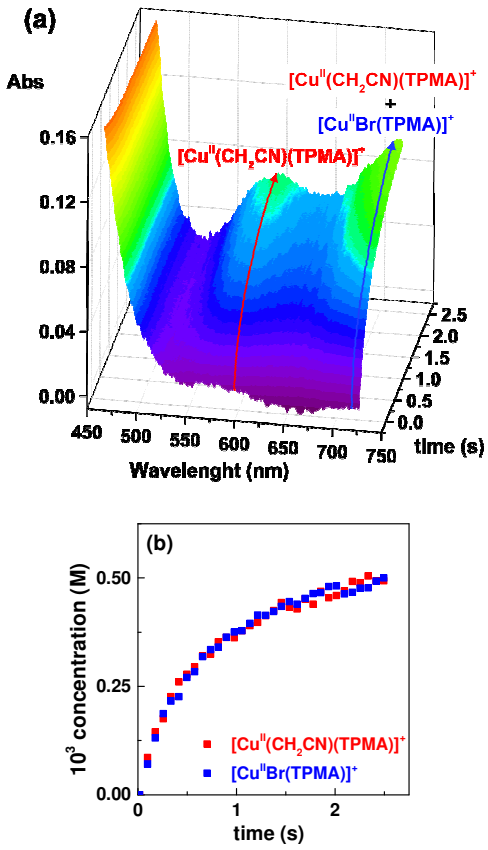

Figure 1. Reaction between 1.2×10^{-3} M $[Cu^{I}(TPMA)]^{+}TfO^{-}$ and 0.6×10^{-3} M BAN in acetonitrile at 25 °C. (a) Evolution of the visible spectrum; the arrows are visual cues to follow the shift of the main spectral features. (b) Experimental evolution of the $[Cu^{II}(CH_2CN)(TPMA)]^{+}$ (red squares) and $[Cu^{II}Br(TPMA)]^{+}$ (blue squares) concentrations with time.

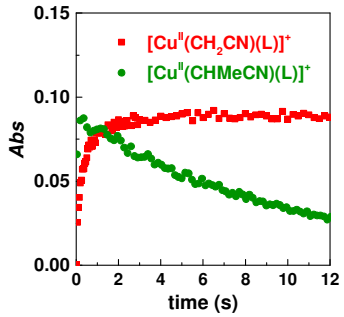

Figure 2. Comparison between the decay of absorbance for $[Cu^{II}(CH_2CN)(TPMA)]^+$ (red squares) and $[Cu^{II}(CHMeCN)(TPMA)]^+$ (green circles). Wavelength = 600 nm. Spectra recorded in acetonitrile at 25 ° C.

Figure 2 shows the evolution of the $[Cu^{II}(CH_2CN)(TPMA)]^+$ concentration on a longer timescale. The organometallic species formed quantitatively and was stable for at least 10 seconds. This indicated that little to no radical termination occurred in this time period due to the relatively high stability of $[Cu^{II}(CH_2CN)(TPMA)]^+$. When the same type of reaction was carried out between $[Cu^{I}(TPMA)]^+TfO^-$ and 2-bromoproprionitrile (BPN), an even faster formation of $[Cu^{II}(CHMeCN)(TPMA)]^+$ was observed (Figure 2), because the ATRP activation of BPN is faster than that of BAN.[26] However, the generated organometallic complex was significantly less stable with an apparent half-lifetime of only 6 s. This is consistent with a lower bond stability between the secondary radical $PN^•$ and the copper ion, as compared to the primary $AN^•$. The $[Cu^{II}(CH_2CN)(TPMA)]^+$ stability was further probed by monitoring the Vis-NIR spectrum on a much longer timescale (Figure S3 and Figure 3); the half-lifetime at 25 ° C was about 3 hours in CH_3CN (Figure 3a) and exceeded 10 h in DMF (Figure 3b). The copper trapping process can stabilize radicals with striking efficiency: given the high reactivity of the $[Cu^{I}(TPMA)]^+$ + BAN system, half of the $AN^•$ radicals would be generated and terminate in less than 0.01 s if they were not trapped by excess $[Cu^{I}(TPMA)]^+$, which instead extends the radical termination process to more than 10 h—a 1,000,000 times difference in radical lifetime (see Figure S4).

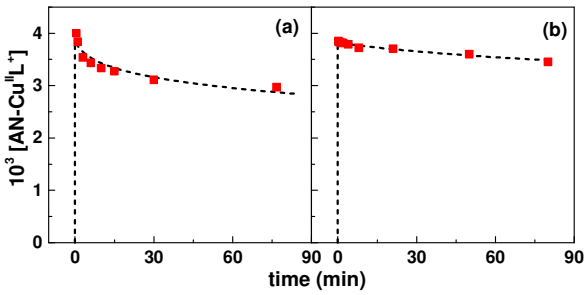

Figure 3. Reaction between 10^{-2} M $[Cu^{I}(TPMA)]^{+}TfO^{-}$ and 5×10^{-3} M BAN at 25 ° C in (a) CH_3CN and (b) DMF. Experimental (squares) and simulated (dashed lines) data of the $[Cu^{II}(CH_2CN)(TPMA)]^{+}$ concentration, on the basis of the mechanism in Scheme 3 as explained below.

These spectroscopic experiments, however, did not provide any kinetic information on the reaction between R$^{\bullet}$ and $[Cu^{I}(TPMA)]^{+}$, because its rate was limited by the relatively slow generation of R$^{\bullet}$ via ATRP activation of RBr. Therefore, these Vis-NIR experiments were combined with electrochemical techniques to further study the formation of the organocopper(II) species.

Electrochemical Analysis of ATRP and OMRP. Three different CV experiments were carried out to obtain quantitative information on the ATRP and OMRP parameters, in the following order of increasing complexity: i) CV of $[Cu^{II}Br(L)]^{+}$ alone; ii) CV of $[Cu^{II}Br(L)]^{+}$ in the presence of RBr and the radical scavenger TEMPO (T$^{\bullet}$); iii) CV of $[Cu^{II}Br(L)]^{+}$ in the presence of RBr without the scavenger. The CV experiments are based on the mechanism in Scheme 4, which is adapted from literature[17] with the addition of the CRT reaction (the full set of reactions is also outlined in Table S1).

The typical voltammetric response recorded for $[Cu^{II}Br(L)]^{+}$ is shown in Figure 4 for L = TPMA in CH_3CN. When no RBr is present, a peak couple is observed (blue line, peaks **A** and **B**), due to the quasi-reversible reduction of $[Cu^{II}Br(TPMA)]^{+}$. The standard reduction potential of this peak couple is denoted as E^{θ}_{Br}.

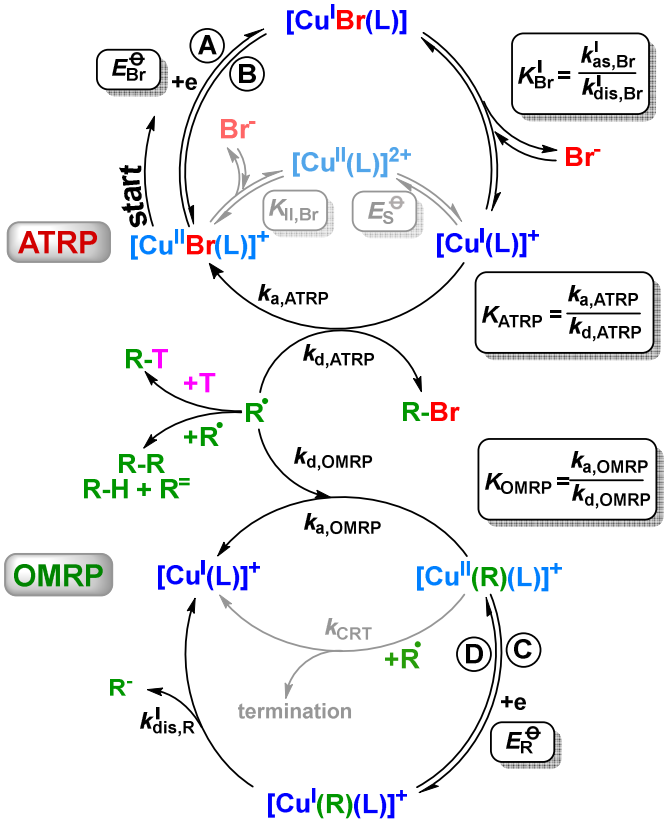

Scheme 4. Mechanism of ATRP and OMRP under electrochemical generation of the active $[Cu^{I}(L)]^{+}$ complex; the segments A, B, C, and D refer to the redox peaks detected in CV experiments.

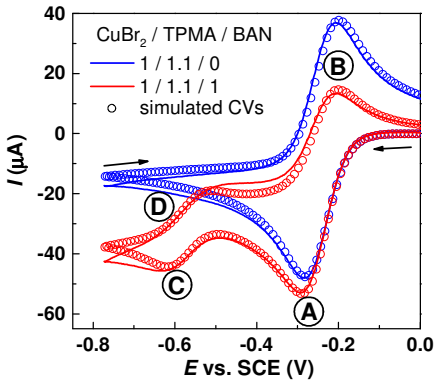

Figure 4. Background-subtracted experimental (lines) and simulated (circles) CVs for 10^{-3} M $Cu^{II}Br_2$ + 1.1 × 10^{-3} M TPMA in CH_3CN + 0.1 M Et_4NBF_4, in the absence (blue) and presence (red) of 10^{-3} M BAN. Scan rate = 0.5 V s^{-1}, T = 25 °C.

In the presence of RBr (Figure 4, red line), the **A/B** peak couple is modified and a second peak couple, **C/D**, appears at more negative potential values. Several additional processes occur in the vicinity of the electrode surface: i) $[Cu^{I}(TPMA)]^{+}$ is electrogenerated and then it reacts with RBr to generate radicals (ATRP activation); ii) $[Cu^{II}Br(TPMA)]^{+}$ reacts with $R^{\bullet}$ to re-generate $[Cu^{I}(TPMA)]^{+}$ and RBr (ATRP deactivation), and iii) $[Cu^{I}(TPMA)]^{+}$ traps $R^{\bullet}$ forming $[Cu^{II}(R)(TPMA)]^{+}$ (OMRP deactivation), so that the set of reactions at the bottom of Scheme 4 can be accessed. The cathodic peak **C** is ascribed to the reduction of $[Cu^{II}(R)(TPMA)]^{+}$ to $[Cu^{I}(R)(TPMA)]$, which is then re-oxidized when the potential scan is reversed (anodic peak **D**). The reduction potential of the redox couple $[Cu^{II}(R)(TPMA)]^{+}/[Cu^{I}(R)(TPMA)]$ ($E_R^{\ominus}$) is more negative than that of $[Cu^{II}Br(TPMA)]^{+}/[Cu^{I}Br(TPMA)]$, i.e. $E_R^{\ominus} < E_{Br}^{\ominus}$, because R is a stronger σ-donor in the organometallic species than Br in the corresponding $[Cu^{II}Br(TPMA)]^{+}$. The electron transfer to $[Cu^{II}(R)(TPMA)]^{+}$ is rather sluggish with a standard rate constant k_R^0 between 0.002 cm s^{-1} and 0.005 cm s^{-1}. The intensity of peak **D** is generally low, possibly because of the dissociation of $[Cu^{I}(R)(TPMA)]$ to R^{-} and $[Cu^{I}(TPMA)]^{+}$ (with rate constant $k_{dis,R}^{I}$), due to the preference of Cu^{I} for a coordination number 4.[17] Completing the return scan, peak **B** is observed with typically a lower current than when RBr is absent, due to the occurrence of both ATRP and OMRP activation/deactivation.

Quantitative information on the kinetics and thermodynamics of ATRP and OMRP can be obtained from computer simulations of the experimental CVs with a suitable model, as proposed by Bernhardt et *al.*.[17, 18] Using the mechanism in Scheme 4, the CVs were successfully fitted by the CV-simulation software DigiElch 8 (Gamry), which is shown in the very good match between experimental data (solid lines) and simulated ones (circles) in Figure 4 and Figure 5. The simulation procedure was used to obtain detailed kinetic information on the organometallic intermediates for the various catalysts and initiators in Scheme 2, including the values of $k_{d,ATRP}$, $k_{d,OMRP}$, $k_{a,OMRP}$, and $k_{dis,R}^{I}$, and the electrochemical parameters $E_R^{\ominus}$ and k_R^0 (i.e. the standard reduction potential and the standard rate constant of the electron transfer for the $[Cu^{II}(R)(L)]^{+}/[Cu^{I}(R)(L)]$ couple). In order to improve the accuracy of the CV simulations, all other parameters in Scheme 4 were determined independently, according to previously reported procedures, as described in detail in Section S3. Moreover, the background capacitive current was subtracted, and the reaction space was thoroughly explored by varying the scan rate and RBr concentration.

ATRP and OMRP Parameters of the TPMA/BAN System. Table 1 shows the ATRP and OMRP parameters for the TPMA/BAN system in CH_3CN and DMF, obtained from the CV simulations. Some representative CVs for these systems, both experimental and simulated, are presented in Figure 4, Figure 5a and S12. Large values of K_{ATRP} and $k_{a,ATRP}$ were determined, in agreement with the high activity of this initiator.[26] The CV in Figure 4 shows the formation of a significant amount of $[Cu^{II}(CH_2CN)(TPMA)]^+$ (peak **C**): once radicals were produced, they quickly reacted with $[Cu^{I}(TPMA)]^+$ to form the organometallic species. Indeed, the simulation returned a very large value for the OMRP trapping, $k_{d,OMRP} = 4.1\times10^7$ M^{-1} s^{-1}. This value agrees with the literature data for the same system.[17] However, the CV simulation could not detect the value of $k_{a,OMRP}$ and K_{OMRP} because $[Cu^{II}(CH_2CN)(TPMA)]^+$ was stable for the time scale of a cyclic voltammetry (> 15 s at the slowest employed scan rate). This agrees with the very slow decay of the organometallic complex detected spectroscopically in Figure 1b. As a consequence, the CV fitting where identical for every $k_{a,OMRP} < 10^{-2}$ M^{-1} s^{-1} (Table S6). Different from the previous investigation,[17] the value of $k_{a,OMRP}$ was too small to be obtained from our CV simulations with sufficient accuracy. Therefore, a different method was used to measure $k_{a,OMRP}$.

Table 1. ATRP and OMRP parameters for the $CuBr_2$/TPMA/BAN system in CH_3CN and DMF.[a]

	CH_3CN	CH_3CN[b]	DMF
K_{Br}^{II} (M^{-1})	3.4×10^7		4.2×10^5
K_{Br}^{I} (M^{-1})	1.9×10^3		1.4×10^4
$k_{as,Br}^{I}$ (M^{-1} s^{-1})[c]	$> 5 \times 10^7$		$> 10^7$
$k_{dis,Br}^{I}$ (s^{-1})[c]	$> 3 \times 10^4$		$> 7 \times 10^2$
K_{ATRP}	$(2.2 \pm 0.7)\times10^{-3}$	3.3×10^{-1}	$(6.7 \pm 1.1)\times10^{-3}$
$k_{a,ATRP}$ (M^{-1} s^{-1})	$(7.75 \pm 0.08)\times10^3$	4.0×10^4	$(4.01 \pm 0.04)\times10^4$
$k_{d,ATRP}$ (M^{-1} s^{-1})	$(3.4 \pm 1.1)\times10^6$	1.2×10^5	$(6.0 \pm 1.1)\times10^6$
K_{OMRP} (M)[d]	$(1.1 \pm 0.3)\times10^{-9}$	4.5×10^{-9}	$(4.2 \pm 1.4)\times10^{-10}$
$k_{a,OMRP}$ (s^{-1})	$(4.6 \pm 0.8)\times10^{-2}$[e]	0.16	$(7.9 \pm 1.9)\times10^{-2}$
$k_{d,OMRP}$ (M^{-1} s^{-1})	$(4.1 \pm 0.6)\times10^7$	3.6×10^7	$(1.9 \pm 0.2)\times10^8$
$k_{dis,R}^{I}$ (s^{-1})	(2.8 ± 0.3)	--	(0.31 ± 0.02)
E_R^e *vs.* SCE (V)	(-0.565 ± 0.004)	-0.569	(-0.495 ± 0.002)
E_{Br}^e - E_R^e (V)	0.323	0.310	0.263
k_R^0 (cm s^{-1})[f]	(0.017 ± 0.009)	--	(0.0018 ± 0.0002)

[a]Errors were estimated at 95% confidence level. [b]From ref.[17]. [c]The lower limit of these rate constant was determined as described in section S3.2; higher values had no effect on the simulated voltammograms. [d]Calculated as $K_{OMRP} = k_{a,OMRP}/k_{d,OMRP}$. [e]Calculated from the decay of $[Cu^{II}(CH_2CN)(TPMA)]^+$ in time (Figure 3). [f]Heterogeneous electron transfer rate constant.

To determine $k_{a,OMRP}$, the stability of $[Cu^{II}(CH_2CN)(TPMA)]^+$ was monitored by UV-visible spectroscopy over a longer period. Figure 3 shows that a rather stable organometallic complex was simply formed by mixing $[Cu^{I}(TPMA)]^+$ and BAN, and that its concentration decreased very slowly. The $[Cu^{II}(CH_2CN)(TPMA)]^+$ decay was fitted with the kinetic simulation program PREDICI[32] (CiT – Computing in Technology, v6.3.2) on the basis of the mechanism in Scheme 3 and the parameters obtained by CV simulation (Table 1), thus leaving only $k_{a,OMRP}$ as an unknown parameter. It should be noted that our simulation did not include transfer of $^{\bullet}CH_2CN$ to solvent.

The PREDICI fitting of the experimental $[Cu^{II}(CH_2CN)(TPMA)]^+$ concentration is presented in Figure 3a,b (dashed lines) for the CH_3CN and DMF solutions. The resulting $k_{a,OMRP}$ value is rather small in both solvents, in the order of 10^{-2} s^{-1}. Such $k_{a,OMRP}$ values would suggest a half-lifetime for the organometallic intermediate ($\ln 2/k_{a,OMRP}$) of $\approx$ 1 minute. The much longer detected lifetime (Figure 3a,b) results from the "persistent radical effect",[33] i.e. $[Cu^{I}(TPMA)]^+$ and $[Cu^{II}Br(TPMA)]^+$ can scavenge the radicals released from $[Cu^{II}(CH_2CN)(TPMA)]^+$, slowing down their termination.

Compared to values previously published by Bernhardt at al.,[17] the combined use of electrochemical and spectrochemical methods in our study resulted in different ATRP parameters and different $k_{a,OMRP}$. The K_{OMRP} value, calculated as $k_{a,OMRP}/k_{d,OMRP}$, is very low, about 10^{-9} M, in both CH_3CN and DMF. This agrees with literature values, as the association between the primary radical $^{\bullet}CH_2CR_2OH$ and $[Cu^{I}(phenantroline)]^+$ was reported with $K_{OMRP} < 10^{-6}$ M and $k_{d,OMRP} \approx 10^{10}$ M^{-1} s^{-1}.[34]

Effect of Initiator on the ATRP and OMRP Parameters. The initiator effect for the $[Cu^{II}Br(TPMA)]^+$ catalyst in DMF solution is presented in Table 2. Representative experimental and simulated CVs are collected in Figure 5 (additional CVs for these systems are shown in Figure S10). A poly(methyl acrylate) macroinitiator (PMA-Br, molecular weight = 2580) was also investigated by CV (Figure 5e and Figure S10e) and found to behave similarly to its small-molecule analogue MBP. The PMA-Br system, however, was characterized by much smaller

currents due to the small diffusion coefficient of the macroinitiator, resulting in lower accuracy of the parameters obtained through the simulation.

The CV simulations correctly captured all expected trends of the ATRP process, which have been extensively investigated in the literature.[26, 35, 36] The ATRP activity (in terms of both K_{ATRP} and $k_{a,ATRP}$) depends on the substituent group, increasing in the order ester < phenyl < cyano. The reactivity increases with the degree of substitution of the C-Br bond, with primary < secondary < tertiary. The ATRP deactivation ($k_{d,ATRP}$) also depends on the radical structure. Secondary radicals are deactivated up to one order of magnitude faster than primary ones, indicating that steric hindrance is not the main factor governing their fast ATRP deactivation. However, the tertiary EiB$^{\bullet}$ radical is deactivated more slowly than the corresponding secondary radical MP$^{\bullet}$, suggesting that steric hindrance plays a larger role in the case of obstructed tertiary radicals.

No organometallic species was detected for the benzylic initiators BBn and PEBn, and for the tertiary EBiB. Bernhardt et *al.* also detected no or very unstable $[Cu^{II}(CMe_2COOEt)(TPMA)]^+$ species for the EBiB case.[17, 18] Conversely, a significant signal for $[Cu^{II}(R)(TPMA)]^+$ was recorded for all other investigated initiators: BAN, BPN, EBA, and MBP. This trend indicates that electrophilic radicals (i.e. nitrile- and ester-stabilized radicals) form much more stable $[Cu^{II}(R)(TPMA)]^+$ species than nucleophilic ones (e.g. styryl radicals). Moreover, hindered tertiary radicals do not bind, or bind much more weakly, to $[Cu^{I}(L)]^+$.

The OMRP equilibrium constants are very small, $K_{OMRP} < 3 \times 10^{-7}$ M, for both primary and secondary electrophilic radicals. Nitrile-stabilized radicals (AN$^{\bullet}$, PN$^{\bullet}$) bind more strongly to $[Cu^{I}(L)]^+$ than ester-stabilized radicals (EA$^{\bullet}$, MP$^{\bullet}$). This agrees with the standard reduction potential of the respective $[Cu^{II}(R)(TPMA)]^+$ ($E_R^{\ominus}$), which is ca 100 mV more negative for nitrile-containing species than for esters, indicating a higher thermodynamic drive for the formation of $[Cu^{II}(CH_2CN)(TPMA)]^+$ and $[Cu^{II}(CHMeCN)(TPMA)]^+$. Moreover, K_{OMRP} is smaller for primary than for secondary radicals. In this case, however, the redox potential is slightly more negative for secondary $[Cu^{II}(R)(TPMA)]^+$.[18]

Table 2. Alkyl halide effect on the ATRP and OMRP parameters for Cu/TPMA in DMF at 25 °C[a]

	BAN	BPN	EBA	MBP	PMA-Br	EBiB[b]	BBn[b]	PEBn[b]
K_{ATRP}	$(6.7 \pm 1.1)\times10^{-3}$	$(1.1 \pm 0.1)\times10^{-2}$	$(2.7 \pm 1.4)\times10^{-6}$	$(1.9 \pm 0.3)\times10^{-5}$	$(4 \pm 3) \times 10^{-5}$	1.8×10^{-3}	2.5×10^{-4}	9.1×10^{-4}
$k_{a,ATRP}$ (M^{-1} s^{-1})	$(4.0 \pm 0.1)\times10^{4}$	$(2.3 \pm 0.1)\times10^{5}$	$(3.9 \pm 0.1)\times10^{1}$	$(3.5 \pm 0.1)\times10^{3}$	$(2.4 \pm 0.3) \times 10^{3}$	3.8×10^{4}	1.2×10^{3}	7.5×10^{3}
$k_{d,ATRP}$ (M^{-1} s^{-1})	$(6.0 \pm 1.1)\times10^{6}$	$(2.0 \pm 0.2)\times10^{7}$	$(1.4 \pm 0.7)\times10^{7}$	$(1.8 \pm 0.3)\times10^{8}$	$(5 \pm 4) \times 10^{7}$	2.2×10^{7}	4.7×10^{6}	8.2×10^{6}

K_{OMRP} (M)	$(4.2 \pm 1.4)\times10^{-10}$[c]	$(2.1 \pm 0.3)\times10^{-8}$	$> 2.0 \times 10^{-8}$	$(2.6 \pm 0.8)\times10^{-7}$	$(1.0 \pm 0.7) \times 10^{-6}$	-	-	-
$k_{a,OMRP}$ (s^{-1})	$(7.9 \pm 1.9)\times10^{-2}$[e]	29 ± 8	< 1[f]	$(3.4 \pm 1.6)\times10^{2}$	$(9 \pm 8) \times 10^{2}$	-	-	-
$k_{d,OMRP}$ (M^{-1} s^{-1})	$(1.9 \pm 0.2)\times10^{8}$	$(1.4 \pm 0.2)\times10^{9}$[d]	$(5.0 \pm 2.6)\times10^{7}$	$(1.3 \pm 0.2)\times10^{9}$[d]	$(0.9 \pm 0.2) \times 10^{9}$	-	-	-
k_{CRT} (M^{-1} s^{-1})	-	-	-	$(9 \pm 5)\times10^{6}$	$(5 \pm 4) \times 10^{6}$	-	-	-
$k^{I}_{dis,R}$ (s^{-1})	0.31 ± 0.02	0.61 ± 0.03	0.28 ± 0.04	$> 10^{2}$ [g]	$> 10^{2}$ [g]	-	-	-
E^{e}_{R} *vs.* SCE (V)	-0.495 ± 0.002	-0.534 ± 0.005	-0.393 ± 0.008	-0.435 ± 0.021	-0.582 ± 0.020	-	-	-
E^{e}_{Br} - E^{e}_{R} (V)	0.263	0.302	0.161	0.203	0.350	-	-	-
k^{0}_{R} (cm s^{-1})	0.0018 ± 0.0002	0.0035 ± 0.0003	0.002 ± 0.011	0.004 ± 0.002	0.004 ± 0.002	-	-	-

[a]Errors were estimated at 95% confidence level. Values for the halidophilicity parameters of the $CuBr_2$/TPMA system in DMF can be found in Table 1. [b]Errors for $k_{a,ATRP} \leq 5\%$, and for K_{ATRP} and $k_{d,ATRP} < 15\%$. [c]Calculated as $K_{OMRP} = k_{a,OMRP}/k_{d,OMRP}$. [d]Diffusion-limited rate constant calculated via the Smoluchowski equation (see Section S3). [e]Calculated from the decay of $[Cu^{II}(CH_2CN)(TPMA)]^+$ vs time (Figure 3). [f]$[Cu^{II}(CH_2COOEt)(TPMA)]^+$ was stable in the timescale of a CV experiment; values of $k_{a,OMRP} < 1$ s^{-1} did not influence the CV simulations. [g]The CV simulations did not change for values larger than 10^2 s^{-1}.

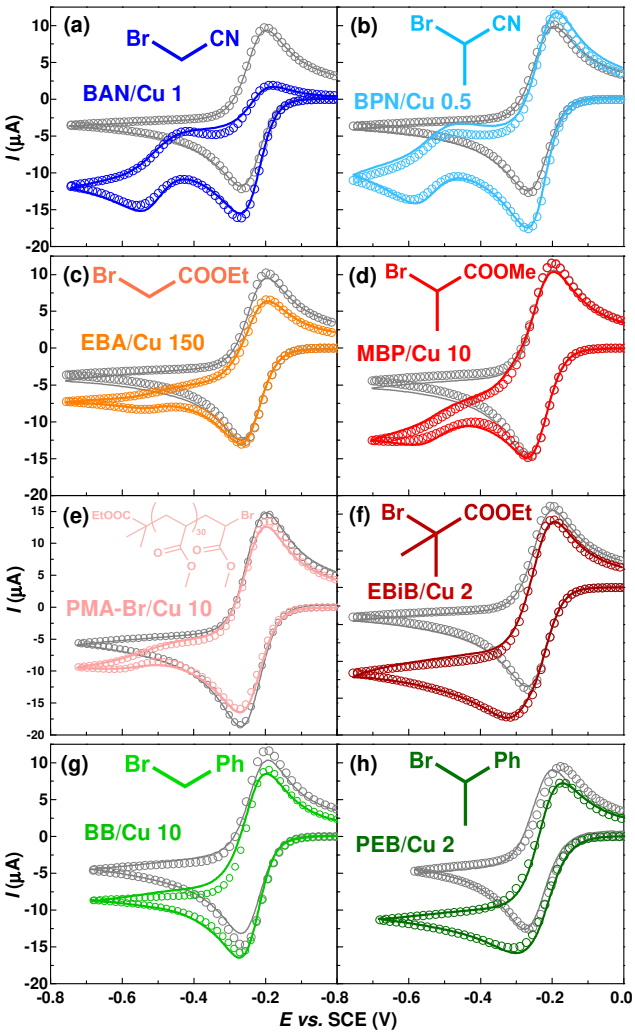

Figure 5. Background-subtracted experimental (solid lines) and simulated (circles) CVs of 10^{-3} M $CuBr_2$ + 1.1 × 10^{-3} M TPMA in DMF + 0.1 M Et_4NBF_4, recorded in the absence and in the presence of RBr. Scan rate = 0.1 V s^{-1}, T = 25 °C (except (e): scan rate = 0.2 V s^{-1} and $CuBr_2$ = 9 × 10^{-4} M in the presence of PMA-Br). [RBr]/[Cu] ratio is indicated in the figures. CVs at all investigated RBr concentrations are presented in Figure S10.

The formation of $[Cu^{II}(R)(TPMA)]^+$ is extraordinarily fast, with $k_{d,OMRP}$ between 10^8 and 10^9 M^{-1} s^{-1}. Ester-based radicals (EA$^\bullet$, MP$^\bullet$) react with a similar rate with respect to the corresponding nitrile-based radicals (AN$^\bullet$, PN$^\bullet$); secondary radicals are trapped faster than primary ones.

In the case of MBP, the best fit of the CV experiments was obtained when $k_{d,OMRP}$ was set to the diffusion limit for a second order reaction (the diffusion-limited rate constant was calculated with the Smoluchowski equation[37, 38] as described in section S3). This suggests that $[Cu^{I}(TPMA)]^{+}$ traps the MP$^{\bullet}$ radical at the fastest possible rate; therefore, it should be able to compete with conventional radical traps such as TEMPO. This hypothesis was confirmed by additional CV simulation in the presence of different amounts of TEMPO (Figure S11).

The RBr nature also had an effect on the $[Cu^{II}(R)(TPMA)]^{+}$ dissociation rate (i.e. OMRP activation, $k_{a,OMRP}$). Primary radicals dissociated from $[Cu^{II}(R)(TPMA)]^{+}$ much more slowly than secondary ones. As discussed in the previous section, the primary cyanoalkyl adduct, $[Cu^{II}(CH_2CN)(TPMA)]^{+}$, is stable in the timescale of the CV experiment;[17] the same is true for the ester-substituted analogue, $[Cu^{II}(CH_2COOEt)(TPMA)]^{+}$. Indeed, the exceptional stability of $[Cu^{II}(CH_2COOEt)(TPMA)]^{+}$ was confirmed by following spectroscopically the reaction between two equivalents of $[Cu^{I}(TPMA)]^{+}$ and one equivalent of EBA in DMF (Figure S15); the organometallic complex was formed quantitatively and then slowly dissociated with a half-lifetime of over 2 h. Conversely, the dissociation of the secondary alkyl adducts $[Cu^{II}(CHMeCN)(TPMA)]^{+}$ and $[Cu^{II}(CHMeCOOMe)(TPMA)]^{+}$ was fast enough to be detected in the CV timescale. This can be qualitatively observed in the CVs in Figure 5b and Figure 5d: the $[Cu^{II}Br(TPMA)]^{+}$/$[Cu^{I}Br(TPMA)]$ peak couple remained reversible in the presence of secondary RBr because $[Cu^{II}(R)(TPMA)]^{+}$ dissociated sufficiently rapidly to reform the original $[Cu^{I}Br(TPMA)]$ complex. Therefore, reliable values of the $[Cu^{II}(R)(TPMA)]^{+}$ dissociation rate constants ($k_{a,OMRP}$) were obtained from CV simulations for both $[Cu^{II}(CHMeCN)(TPMA)]^{+}$ and $[Cu^{II}(CHMeCOOMe)(TPMA)]^{+}$.

Overall, the OMRP equilibrium is less "dynamic" for primary ATRP initiators, while secondary RBr are both activated and deactivated faster. The same was found for the ATRP equilibrium, in several solvents.[18, 26]

The Contribution of Catalyzed Radical Termination. Before discussing the effect of the multidentate N-based ligand (L) on the formation of organometallic species, it is necessary to evaluate alternative decomposition pathways for the organometallic species. It was previously shown that $[Cu^{II}(R)(L)]^{+}$ can promote radical termination reactions: $[Cu^{II}(R)(L)]^{+} + R^{\bullet} \rightarrow [Cu^{I}(L)]^{+}$ + terminated chains (Scheme 1, blue box).[39] Since this process regenerates the Cu^{I} complex, which can then trap a new radical, the overall result is a Cu-catalyzed radical termination (CRT). The

CRT was therefore included in our analysis as shown in Scheme 3 and Scheme 4. The use of anhydrous solvents prevented other decomposition pathways of $[Cu^{II}(R)(L)]^+$, which involve the presence of proton donors as shown in other contribution.[22,40]

No significant contribution of CRT was apparent in the case of nitriles, neither in the CV nor in the Vis-NIR spectroscopic experiments: introduction of this process into the CV simulation did not significantly improve the quality of the fit, which returned a negligible value of k_{CRT}; moreover, the Vis-NIR kinetics of decomposition of $[Cu^{II}(CH_2CN)(TPMA)]^+$ could be accurately modeled without accounting for any CRT reaction, as shown above in Figure 3.

CV simulations for the case of MBP where first carried out without considering the CRT reaction, which yielded the ATRP and OMRP parameters in Table S7. The accuracy of those values was tested by the following orthogonal experiment. Mixing $Cu^{I}OTf$/TPMA with MBP in a 2:1 ratio generated $[Cu^{II}Br(TPMA)]^+$ and $[Cu^{II}(CHMeCOOMe)(TPMA)]^+$ (Scheme 3). The accumulation and decay of these Cu^{II} species was monitored by Vis-NIR spectroscopy (Figure 6a). In Figure 6b, the resulting concentration of $[Cu^{II}Br(TPMA)]^+$ and estimated concentration of $[Cu^{II}(CHMeCOOMe)(TPMA)]^+$ are plotted in filled and hollow squares, respectively. Then, the concentration vs time plot was simulated using the software PREDICI,[32] in agreement with the set of reactions in Scheme 3 and the thermodynamic and kinetic parameters in Table S7 (obtained from electrochemistry without considering CRT). The simulated data did not match the experimental ones (red lines).

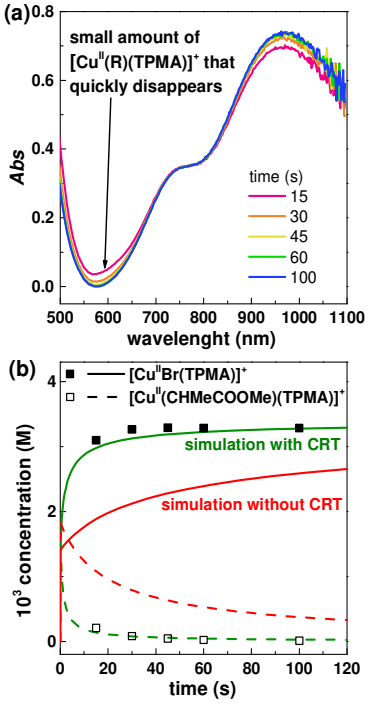

Figure 6. "Termination" experiment between 8×10^{-3} M $[Cu^{I}(TPMA)]^{+}$ and 4×10^{-3} M MBP in DMF at 25 °C. (a) Vis-NIR spectra. (b) Experimental and simulated $[Cu^{II}Br(TPMA)]^{+}$ and $[Cu^{II}(CHMeCOOMe)(TPMA)]^{+}$ using data from electrochemistry (Table 2). The complete set of equations used in the simulation is presented in Table S8. The concentration of $[Cu^{II}(R)(L)]^{+}$ was estimated by using ε = 162 $L\cdot mol^{-1}\cdot cm^{-1}$ at 600 nm obtained for $[Cu^{II}(CH_2COOEt)(TPMA)]^{+}$ in Figure S15.

Therefore, the CRT reaction, which is known to affect secondary acrylate radicals, was added to the model for the CV simulation. The fitting of experimental CV slightly improved, yielding k_{CRT} = 9×10^{6} M^{-1} s^{-1} for the reaction between $[Cu^{II}(CHMeCOOMe)(TPMA)]^{+}$ and $^{\bullet}$CHMeCOOMe. The corresponding ATRP and OMRP parameters are listed in Table 2. Then, the dataset with inclusion of k_{CRT} was used to simulate the same orthogonal Vis-NIR experiment in Figure 6a, and the agreement between experimental and simulated concentration of $[Cu^{II}Br(TPMA)]^{+}$ was good (Figure 6b, green lines). This suggested that the CRT reaction plays an important role in the termination of MBP-derived radicals.

The ORMP and CRT parameters in the case of the macroinitiator PMA-Br were similar to those of the small-molecule analogue MBP. In the case of EBA, $[Cu^{II}(CH_2COOEt)(TPMA)]^{+}$ was stable in the timescale of the CV experiment, which prevented the determination of $k_{a,OMRP}$ and

(potential) k_{CRT} values. Thus, only an upper-limit estimate of $k_{a,OMRP}$ is given in Table 2. Finally, in the cases of EBiB and phenyl-substituted radicals, no organocopper species could be detected, and thus also no CRT. In contrast, iron catalysts strongly react with both tertiary and phenyl-substituted radicals.[41, 42]

Effect of Catalyst on the ATRP and OMRP Parameters. Table 3 reports the results of CV simulation for three catalysts of the TPMA family (structures in Scheme 2), with the initiator MBP in DMF. The ligands have similar structures but very different electronic properties due to the contribution of electron-donating groups, which alter their ATRP reactivity. Values of $k_{a,ATRP}$ greatly increase in the order TPMA < TPMA*[3] < TPMA^{NMe2}, in line with literature reports.[43, 44] In addition, the ATRP deactivation rate constant slightly decreases along the same series. Overall, the K_{ATRP} increases over 4 orders of magnitude when switching from Cu/TPMA to the most reactive Cu/TPMA^{NMe2}. The K_{OMRP} value is much less affected by the catalyst nature: the more active catalysts, Cu/TPMA*[3] and Cu/TPMA^{NMe2}, show only 20-30 times smaller K_{OMRP} than the less active Cu/TPMA. This trend agrees with previously reported DFT calculations.[20]

Cu/TPMA*[3] and Cu/TPMA^{NMe2} yield slower OMRP kinetics (both activation, $k_{a,OMRP}$, and deactivation, $k_{d,OMRP}$) than Cu/TPMA. Therefore, the classic Cu/TPMA scaffold quickly reacts with radicals, while Cu/TPMA*[3] presents the highest affinity (lowest K_{OMRP}) towards MP$^{\bullet}$. This agrees with E_R^{θ} being the most negative for the Cu/TPMA*[3] system.

Table 3. Ligand effect on the formation of the organometallic species from $Cu^{II}Br_2$/L and MBP in DMF.[a]

	TPMA	TPMA*3	TPMA^{NMe2}
K_{Br}^{II} (M^{-1})	4.2×10^5	4.2×10^5	1.2×10^5
K_{Br}^{I} (M^{-1})	1.4×10^4	3.6×10^3	2.5×10^2
$k_{as,Br}^{I}$ (M^{-1} s^{-1})[b]	$> 10^7$	$> 10^8$	$> 5 \times 10^8$
$k_{dis,Br}^{I}$ (s^{-1})[b]	$> 7 \times 10^2$	$> 3 \times 10^4$	$> 2 \times 10^6$
K_{ATRP}	$(1.9 \pm 0.3) \times 10^{-5}$	$(6.5 \pm 0.8) \times 10^{-3}$	$(3.1 \pm 0.6) \times 10^{-1}$
$k_{a,ATRP}$ (M^{-1} s^{-1})	$(3.5 \pm 0.1) \times 10^3$	$(2.6 \pm 0.1) \times 10^5$	$(4.8 \pm 0.3) \times 10^6$
$k_{d,ATRP}$ (M^{-1} s^{-1})	$(1.8 \pm 0.4) \times 10^8$	$(4.0 \pm 0.6) \times 10^7$	$(1.6 \pm 0.4) \times 10^7$
K_{OMRP} (M)	$(2.6 \pm 0.8) \times 10^{-7}$	$(1.0 \pm 0.2) \times 10^{-8}$	$(1.2 \pm 0.2) \times 10^{-8}$
$k_{a,OMRP}$ (s^{-1})	$(3.4 \pm 1.6) \times 10^2$	0.80 ± 0.20	2.3 ± 0.7
$k_{d,OMRP}$ (M^{-1} s^{-1})	$(1.3 \pm 0.2) \times 10^9$	$(8.0 \pm 0.8) \times 10^7$	$(2.0 \pm 0.3) \times 10^8$
k_{CRT} (M^{-1} s^{-1})	$(9 \pm 5) \times 10^6$	$(3 \pm 2) \times 10^5$	$(8 \pm 4) \times 10^5$

$k^{I}_{dis,R}$ (s^{-1})	> 10^{2} [c]	0.12 ± 0.04	2.0 ± 0.4
$\boldsymbol{E^{e}_{R}}$ vs SCE (V)	-0.435 ± 0.021	-0.252 ± 0.005	-0.221 ± 0.006
E^{e}_{Br} - E^{e}_{R} (V)	0.203	0.272	0.245
k^{0}_{R} (cm s^{-1})	0.004 ± 0.002	0.0014 ± 0.0003	0.003 ± 0.001

[a]Errors were estimated at 95% confidence level. [b]The lower limit of the rate constant was determined as described in Section S3; higher values had no effect on the simulated voltammograms. [c]The CV simulations did not change for values larger than 10^{2} s^{-1}.

The CV simulations gave k_{CRT} values > 10^{5} M^{-1} s^{-1} for all ligands, with Cu/TPMA appearing as the fastest to promote this additional termination reaction. However, the effect of k_{CRT} on the CV shape was rather small, so that the standard deviation on this parameter is larger than for the others. The value of k_{CRT} for the Cu/TPMA*[3] system was also confirmed spectroscopically by following the decay of $[Cu^{II}(CHMeCOOMe)(TPMA*^{3})]^{+}$ (Figure S14).

Effect of Solvent on the ATRP and OMRP Parameters. The $CuBr_2$/TPMA + MBP system was investigated in four polar solvents. The CV simulations yielded increasing K_{ATRP} values in the order CH_3CN < DMF < DMSO, in agreement with several previous reports.[38, 45] The value of $k_{d,ATRP}$ is slightly lower in the most ATRP-active solvent, DMSO. K_{OMRP} is in the order of 10^{-6}-10^{-7} M^{-1} in all solvents, and the formation of $[Cu^{II}(CHMeCOOMe)(TPMA)]^{+}$ is very fast, with diffusion-limited or only slightly lower $k_{a,OMRP}$ values. E^{e}_{R} is most negative in CH_3CN, but does not show any particular trend in the other solvents.

The formation of the organometallic species was also investigated in water. A stable and reversible signal for the organometallic complex was detected at all scan rates and MBP concentrations (Figure S13c). This indicated that the protonolysis of $[Cu^{II}(CHMeCOOMe)(TPMA)]^{+}$ is relatively slow. A negligible effect of the addition of small amounts of water on the stability of $[Cu^{II}(CH_2CN)(TPMA)]^{+}$ in CH_3CN was previously reported. It should be noted, however, that the quality of our CV in water was poor, so it was not possible to obtain reliable parameters from the simulations.

Table 4. Solvent effect on the formation of the organometallic species from $Cu^{II}Br_2$/TPMA and MBP.[a]

	CH_3CN	DMF	DMSO
K^{II}_{Br} (M^{-1})	3.4×10^{7}	4.2×10^{5}	1.0×10^{5}
K^{I}_{Br} (M^{-1})	1.9×10^{3}	1.4×10^{4}	4.4×10^{4}

$k^{I}_{as,Br}$ (M^{-1} s^{-1})[b]	> 5×10^7	> 10^7	> 10^7
$k^{I}_{dis,Br}$ (s^{-1})[b]	> 3×10^4	> 7×10^2	> 2×10^3
K_{ATRP}	$(3.5 \pm 0.4) \times 10^{-6}$ [c]	$(1.9 \pm 0.3) \times 10^{-5}$	$(1.3 \pm 0.4) \times 10^{-4}$
$k_{a,ATRP}$ (M^{-1} s^{-1})	$(4.7 \pm 0.1) \times 10^2$	$(3.5 \pm 0.1) \times 10^3$	$(8.7 \pm 0.2) \times 10^3$
$k_{d,ATRP}$ (M^{-1} s^{-1})	$(1.3 \pm 0.2) \times 10^8$	$(1.8 \pm 0.4) \times 10^8$	$(6.7 \pm 2.2) \times 10^7$
K_{OMRP} (M)	$(2.7 \pm 1.4) \times 10^{-6}$	$(2.6 \pm 0.8) \times 10^{-7}$	$(1.1 \pm 0.2) \times 10^{-6}$
$k_{a,OMRP}$ (s^{-1})	$(3 \pm 2) \times 10^2$	$(3.4 \pm 1.6) \times 10^2$	$(6.4 \pm 2.4) \times 10^2$
$k_{d,OMRP}$ (M^{-1} s^{-1})	$(1.1 \pm 0.6) \times 10^8$	$(1.3 \pm 0.2) \times 10^9$	$(5.8 \pm 1.2) \times 10^8$
k_{CRT} (M^{-1} s^{-1})	$(2 \pm 1) \times 10^7$	$(9 \pm 5) \times 10^6$	$(4 \pm 2) \times 10^6$
$k^{I}_{dis,R}$ (s^{-1})	> 10^2 [d]	> 10^2 [d]	12 ± 2
E^{e}_{R} *vs.* SCE (V)	-0.521 ± 0.026	-0.435 ± 0.021	-0.494 ± 0.011
E^{e}_{Br} - E^{e}_{R} (V)	0.279	0.203	0.271
k^{0}_{R} (cm s^{-1})	0.004 ± 0.002	0.004 ± 0.002	0.005 ± 0.002

[a]Errors were estimated at 95% confidence level. [b]Lower limit of rate constant determined as described in Section S3; higher values had no effect on the simulated voltammograms. [c]from ref. [36] [d]The CV simulations did not change for values larger than 10^2 s^{-1}.

The Role of $[Cu^{II}(R)(L)]^+$ in the ATRP of Methyl Acrylate. To clarify the role of organometallic species and CRT under typical polymerization conditions, we conducted PREDICI simulation of a normal ATRP of MA catalyzed by $Cu^{I}Br$/TPMA in CH_3CN, in agreement with the set of reactions in Table S9. It was considered that the chain end of PMA-Br had the same ATRP and OMRP activity as the small-molecule analogue MBP.[46] Moreover, both ATRP and OMRP parameters calculated in pure solvents were considered regardless of the presence of the monomer. Only the polymerization of MA was considered because CRT was not detected for the other investigated systems. It should be noted that under polymerization conditions the radical concentration is lower than under our electrochemical or spectrochemical experiments; therefore, other termination pathways may become more important. Only RT and CRT are considered in the following simulations.

Figure 7a shows the simulated concentration of the most important species during polymerization for the TPMA system. The concentration of organometallic species $[Cu^{II}(R)(TPMA)]^+$ + $[Cu^{II}(P_n)(TPMA)]^+$ (with P_n indicating a polymer chain) was more than 100 times smaller than that of $[Cu^{I}(TPMA)]^+$. However, the contribution of CRT was noticeable, accounting for 92% of total termination. This agrees with the experimental results for MA polymerization, for which 89 to 97% of termination occurred by the CRT process in the presence of Cu/TPMA or other catalysts with similar reactivity.[19]

Figure 7c shows the simulated rates for all relevant reactions occurring during the normal ATRP of MA. The rate of CRT is at least 10 times higher than the rate of bimolecular radical termination. Moreover, the rates of ATRP activation and deactivation closely match, indicating that the ATRP equilibrium is fully established. The same holds true for the OMRP equilibrium. However, the rate of the OMRP exchange between living and dormant species is at least 10 times slower than that of the ATRP exchange. This indicates that most of the polymerization control is due to the faster ATRP activation/deactivation.

In summary, the presence of organometallic intermediates, albeit in low quantity, could increase the termination rate of MA in ATRP by a factor of >10. Polymerization control is largely due to the ATRP equilibrium.

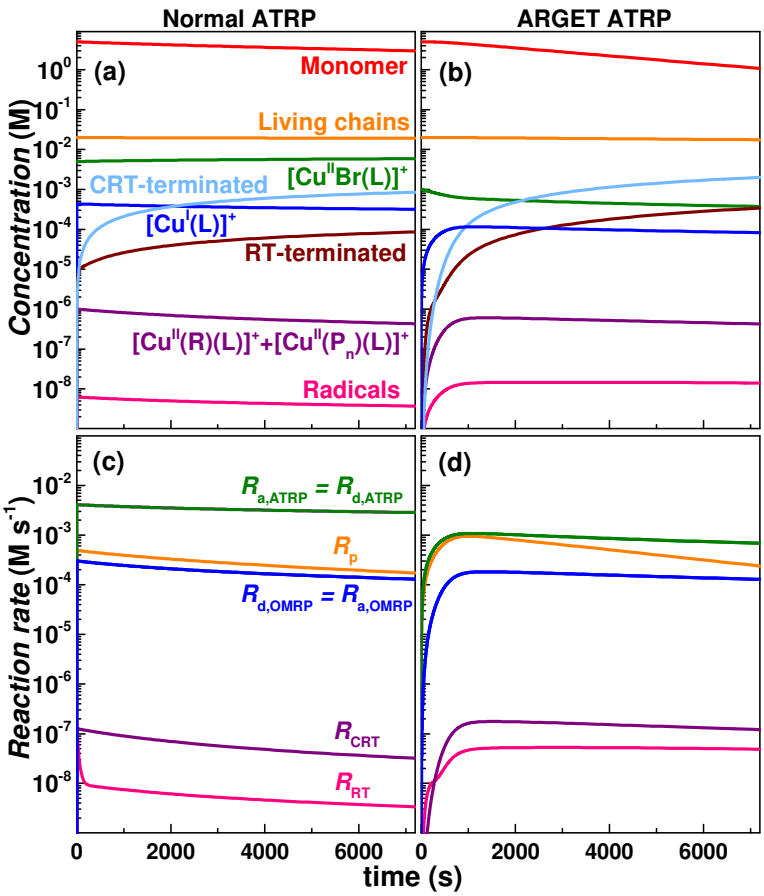

Figure 7. (a,c) Normal ATRP, and (b,d) ARGET ATRP of MA in CH_3CN: (a,b) simulated concentrations of relevant species and (c,d) rates of reactions. L = TPMA, [MA] = 5 M in CH_3CN (45 vol%). Other conditions: (a,c) [MA]:[MBP]:[$Cu^{I}Br$/TPMA]:[$Cu^{II}Br_2$/TPMA] =

250:1:0.25:0.25. Conversion after 2h: 40%, $Đ = 1.03$; (b,d) [MA]:[MBP]:[$Cu^{II}Br_2$/TPMA]:[Sn(II)] = 250:1:0.05:0.25. Conversion after 2h: 79%, $Đ = 1.04$.

Next, we simulated an Activators Regenerated by Electron Transfer (ARGET) ATRP of MA in CH_3CN. In ARGET systems the Cu complexes are present at lower concentrations. The active $[Cu^{I}(L)]^+$ is continuously regenerated during polymerization by reducing agents such as Sn^{II} compounds.[47, 48] Diminishing the amount of copper 5 times via the ARGET process suppressed the contribution of CRT compared to bimolecular radical termination (RT): in the ARGET ATRP process CRT was half as prominent with respect to RT (Figure 7c,d). The rate of the OMRP exchange between radical deactivation and activation remained about 10 times slower than the ATRP exchange. Thus, ATRP was the main reaction controlling radical chain growth.

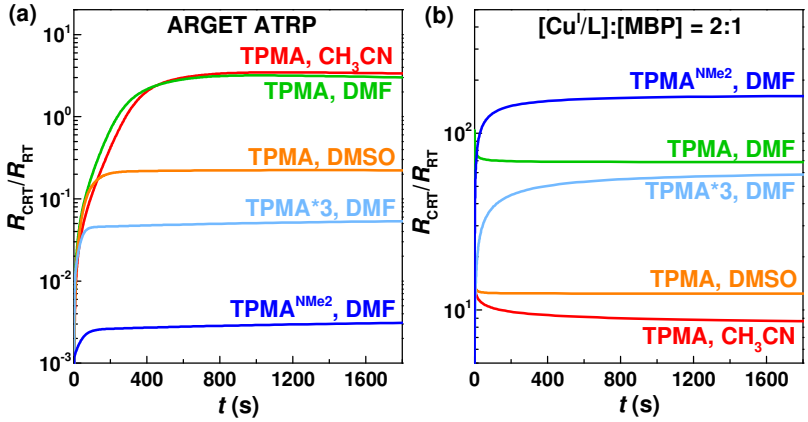

Figure 8. Ratio between the rate of CRT and RT in (a) ARGET ATRP of MA ([MA] = 5 M; [MA]:[MBP]:[$Cu^{II}Br_2$/L]:[Sn^{II}] = 250:1:0.05:0.25), and (b) reaction between 8×10^{-3} M Cu^{I}OTf/L and 4×10^{-3} M MBP, with different catalysts and in different solvents, determined by PREDICI simulation (details on the simulations are presented in Figures S13-S27).

In Figure 8, we analyzed the contribution of CRT by plotting the R_{CRT}/R_{RT} ratios, obtained by PREDICI simulations, for two extreme cases: in Figure 8a, a small amount of $[Cu^{I}(L)]^+$, sub-stoichiometric to RBr, was slowly (re)generated in the ARGET process; in Figure 8b, $[Cu^{I}(L)]^+$ and MBP were reacted in a 2:1 ratio to produce the maximum amount of $[Cu^{II}(R)(L)]^+$.

In the ARGET ATRP case (Figure 8a), the contribution of CRT was suppressed by switching to either more ATRP-active catalysts (e.g. Cu/$TPMA^{NMe2}$) or more ATRP-active solvents (e.g. DMSO). These conditions induced a lower equilibrium concentration of $[Cu^{I}(L)]^+$

and $[Cu^{II}(R)(L)]^+$, which in turn diminished the importance of CRT. For the same reasons, the rates of OMRP activation and deactivation were much slower for the most ATRP-active systems (Figure S30).

Interestingly, mixing $[Cu^{I}(L)]^+$ and MBP in a 2:1 ratio (Figure 8b) resulted in an opposite trend of R_{CRT}/R_{RT} compared to the ARGET ATRP case. When $[Cu^{I}(L)]^+$ and RBr were directly mixed at high concentrations, the most ATRP-active systems generated the highest radical concentration. Then, radicals bonded to $[Cu^{I}(L)]^+$ to form a greater amount of $[Cu^{II}(R)(L)]^+$ species, which promoted CRT.

Conclusions

We have investigated the stability of organometallic species, their rate of formation and disappearance, and their effect on ATRP reactions, by applying spectroscopic and electrochemical techniques. The OMRP and ATRP equilibrium constants are summarized in Figure 9. The stability of organometallic species (which is inversely proportional to K_{OMRP}) strongly depended on the degree of substitution of the radical center, following the order 1° > 2° > 3° (no $[Cu^{II}(R)(L)]^+$ was observed in the latter case). Regarding the nature of the radical, the stability depends on the stabilizing groups in the following order: cyano > esters > phenyl (no $[Cu^{II}(R)(L)]^+$ was observed in the latter case). For the different initiating systems, K_{OMRP} scales directly with K_{ATRP}.

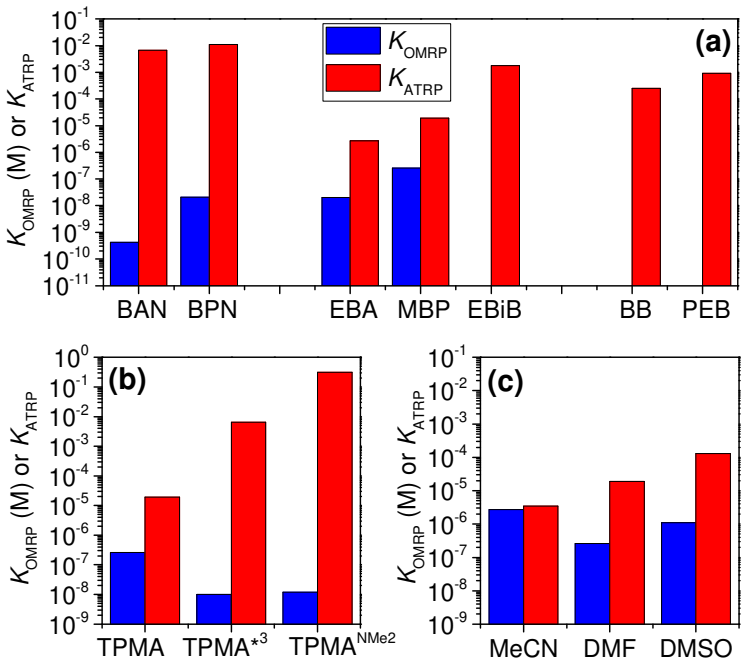

Figure 9. Comparison of ATRP and OMRP equilibrium constants: (a) effect of initiator for the Cu/TPMA system in DMF; (b) effect of copper ligand for the MBP activation in DMF; (c) effect of solvent for the Cu/MBP/TPMA system.

Conversely, for the same MBP initiator K_{OMRP} decreased as the ATRP activity (K_{ATRP}) increased upon varying the nature of the ligand. However, the K_{OMRP} variations are much smaller than those of K_{ATRP}, and similar values were obtained for the two most active catalysts with TPMA*[3] and TPMA^{NMe2} ligands. Moreover, there is no clear trend in K_{OMRP} when changing the solvent, although DMF stabilizes $[Cu^{II}(R)(L)]^+$ the most. The solvent affects K_{ATRP} more than it affects K_{OMRP}. Good stability of the organometallic species was also observed in water, at least at the timescale of the CV experiment, suggesting that their protonolysis is a relatively slow process.

$[Cu^{I}(L)]^+$ traps radicals very efficiently, with diffusion-controlled rates in the case of certain secondary radicals. Compared to the primary radicals, the secondary ones are both trapped faster by $[Cu^{I}(L)]^+$ and dissociate faster from $[Cu^{II}(R)(L)]^+$. This makes the OMRP equilibrium faster—or more "dynamic"—for secondary radicals. The same is true for the ATRP equilibrium. CRT should only be an issue in ATRP of acrylates and possibly acrylamides, while acrylonitrile, methacrylates, methacrylamides and styrenics seem immune from this process. Acrylate-type

radicals displayed k_{CRT} values in the order of 10^5 to 10^7 M^{-1} s^{-1} for the reaction between $[Cu^{II}(R)(L)]^+$ and $R^\bullet$.

Simulations of polymerizations showed that the OMRP equilibrium adds another layer of "control" thanks to the fast activation and deactivation. However, the OMRP exchange was always slower than the ATRP activation/deactivation, by at least one order of magnitude. Nevertheless, copper catalysts for OMRP may be accessed by appropriate modification of the TPMA scaffold.

When the radical concentration is high (e.g. when mixing $Cu^{I}OTf$/TPMA and BAN), the excess $[Cu^{I}(L)]^+$ reversibly traps radicals by forming $[Cu^{II}(R)(L)]^+$; this slows down bimolecular radical termination. This "radical buffering" system might be an important feature in ATRP systems with heterogeneous generation of the activator catalyst (e.g. *e*ATRP[30] or mechanoATRP[49]), where high $[Cu^{I}(L)]^+$ and $R^\bullet$ concentrations can be found at the interface between the polymerization solution and electrode surfaces or piezoelectric surfaces.

CRT is most important for ATRP systems with lower activity (i.e. lower K_{ATRP}), such as Cu/TPMA in CH_3CN or DMF. The contribution of CRT can be diminished by increasing the ATRP activity, which can be accomplished by either changing solvent or ligand. At equilibrium, more ATRP-active systems produce a lower $[Cu^{I}(L)]^+$ concentration, which in turn results in a lower $[Cu^{II}(R)(L)]^+$ concentration, and thus slower CRT.

Author information

Corresponding author

*matyjaszewski@andrew.cmu.edu

ORCID

Marco Fantin: 0000-0001-9581-2076

Francesca Lorandi: 0000-0001-5253-8468

Grzegorz Szczepaniak: 0000-0002-0355-9542

Abdirisak A. Isse: 0000-0003-0966-1983

Rinaldo Poli: 0000-0002-5220-2515

Krzysztof Matyjaszewski: 0000-0003-1960-3402

Author Contributions

‡M.F. and F.L. contributed equally.

Present Address

T.G.R: Avery Dennison Corporation, Chemical Division, 171 Draketown Rd, Mill Hall, PA 17751, United States

Supporting Information

Experimental section, additional CVs, details on PREDICI and electrochemical simulations.

Acknowledgments

Support from the U.S. National Science Foundation (NSF, grant CHE 1707490) and from the French "Centre National de la Recherche Scientifique" (CNRS) through funding of the International Associated Laboratory "Laboratory of Coordination Chemistry for Controlled Radical Polymerization" (LCC-CRP) is gratefully acknowledged. G.S gratefully acknowledges the Polish Ministry of Science and Higher Education ("Mobilnosc Plus" grant no. 1646/MOB/V/2017/0) for financial support.

References

1. Matyjaszewski, K. Advanced Materials by Atom Transfer Radical Polymerization. *Adv. Mater.* **2018,** 30, 1706441.
2. Debuigne, A.; Poli, R.; Jérôme, C.; Jérôme, R.; Detrembleur, C. Overview of cobalt-mediated radical polymerization: Roots, state of the art and future prospects. *Prog. Polym. Sci.* **2009,** 34, 211-239.
3. Ouchi, M.; Terashima, T.; Sawamoto, M. Transition metal-catalyzed living radical polymerization: Toward perfection in catalysis and precision polymer synthesis. *Chem. Rev.* **2009,** 109, 4963-5050.
4. Matyjaszewski, K. Atom Transfer Radical Polymerization (ATRP): Current Status and Future Perspectives. *Macromolecules* **2012,** 45, 4015-4039.
5. Wang, J.-S.; Matyjaszewski, K. Controlled/"living" radical polymerization. atom transfer radical polymerization in the presence of transition-metal complexes. *J. Am. Chem. Soc.* **1995,** 117, 5614-5615.
6. Anastasaki, A.; Nikolaou, V.; Nurumbetov, G.; Wilson, P.; Kempe, K.; Quinn, J. F.; Davis, T. P.; Whittaker, M. R.; Haddleton, D. M. Cu(0)-Mediated Living Radical Polymerization: A Versatile Tool for Materials Synthesis. *Chem. Rev.* **2016,** 116, 835-877.
7. Pan, X.; Fantin, M.; Yuan, F.; Matyjaszewski, K. Externally controlled atom transfer radical polymerization. *Chem. Soc. Rev.* **2018,** 47, 5457-5490.
8. Ribelli, T. G.; Lorandi, F.; Fantin, M.; Matyjaszewski, K. Atom Transfer Radical Polymerization: Billion Times More Active Catalysts and New Initiation Systems. *Macromol. Rapid Commun.* **2019,** 40, 1800616.

9. Allan, L. E. N.; Perry, M. R.; Shaver, M. P. Organometallic mediated radical polymerization. *Prog. Polym. Sci.* **2012,** 37, 127-156.
10. Poli, R. New Phenomena in Organometallic-Mediated Radical Polymerization (OMRP) and Perspectives for Control of Less Active Monomers. *Chem. Eur. J.* **2015,** 21, 6988-7001.
11. Debuigne, A.; Jérôme, C.; Detrembleur, C. Organometallic-mediated radical polymerization of 'less activated monomers': Fundamentals, challenges and opportunities. *Polymer* **2017,** 115, 285-307.
12. Le Grognec, E.; Claverie, J.; Poli, R. Radical Polymerization of Styrene Controlled by Half-Sandwich Mo(III)/Mo(IV) Couples: All Basic Mechanisms Are Possible. *J. Am. Chem. Soc.* **2001,** 123, 9513-9524.
13. Poli, R. Relationship between One-Electron Transition-Metal Reactivity and Radical Polymerization Processes. *Angew. Chem. Int. Ed.* **2006,** 45, 5058-5070.
14. Allan, L. E. N.; Macdonald, J. P.; Nichol, G. S.; Shaver, M. P. Single component iron catalysts for atom transfer and organometallic mediated radical polymerizations: Mechanistic studies and reaction scope. *Macromolecules* **2014,** 47, 1249-1257.
15. Matyjaszewski, K.; Woodworth, B. E. Interaction of Propagating Radicals with Copper(I) and Copper(II) Species. *Macromolecules* **1998,** 31, 4718-4723.
16. Soerensen, N.; Schroeder, H.; Buback, M. SP–PLP–EPR Measurement of CuII-Mediated ATRP Deactivation and CuI-Mediated Organometallic Reactions in Butyl Acrylate Polymerization. *Macromolecules* **2016,** 49, 4732-4738.
17. Zerk, T. J.; Bernhardt, P. V. Organo-Copper(II) Complexes as Products of Radical Atom Transfer. *Inorg. Chem.* **2017,** 56, 5784-5792.
18. Zerk, T. J.; Gahan, L. R.; Krenske, E. H.; Bernhardt, P. V. The fate of copper catalysts in atom transfer radical chemistry. *Polym. Chem.* **2019,** 10, 1460-1470.
19. Wang, Y.; Soerensen, N.; Zhong, M.; Schroeder, H.; Buback, M.; Matyjaszewski, K. Improving the "Livingness" of ATRP by Reducing Cu Catalyst Concentration. *Macromolecules* **2013,** 46, 683-691.
20. Ribelli, T. G.; Wahidur Rahaman, S. M.; Daran, J.-C.; Krys, P.; Matyjaszewski, K.; Poli, R. Effect of Ligand Structure on the CuII–R OMRP Dormant Species and Its Consequences for Catalytic Radical Termination in ATRP. *Macromolecules* **2016,** 49, 7749-7757.
21. Wahidur Rahaman, S. M.; Matyjaszewski, K.; Poli, R. Cobalt(iii) and copper(ii) hydrides at the crossroad of catalysed chain transfer and catalysed radical termination: a DFT study. *Polym. Chem.* **2016,** 7, 1079-1087.
22. Nakamura, Y.; Ogihara, T.; Yamago, S. Mechanism of Cu(I)/Cu(0)-Mediated Reductive Coupling Reactions of Bromine-Terminated Polyacrylates, Polymethacrylates, and Polystyrene. *ACS Macro Lett.* **2016,** 5, 248-252.
23. Nakamura, Y.; Lee, R.; Coote, M. L.; Yamago, S. Termination Mechanism of the Radical Polymerization of Acrylates. *Macromol. Rapid Commun.* **2016,** 37, 506-513.
24. Bell, C. A.; Bernhardt, P. V.; Monteiro, M. J. A rapid electrochemical method for determining rate coefficients for copper-catalyzed polymerizations. *J. Am. Chem. Soc.* **2011,** 133, 11944-11947.
25. Zerk, T. J.; Bernhardt, P. V. New Method for exploring deactivation kinetics in copper-catalyzed atom-transfer-radical reactions. *Inorg. Chem.* **2014,** 53, 11351-11353.
26. Fantin, M.; Isse, A. A.; Bortolamei, N.; Matyjaszewski, K.; Gennaro, A. Electrochemical approaches to the determination of rate constants for the activation step in atom transfer radical polymerization. *Electrochim. Acta* **2016,** 222, 393-401.

27. Fantin, M.; Isse, A. A.; Matyjaszewski, K.; Gennaro, A. ATRP in Water: Kinetic Analysis of Active and Super-Active Catalysts for Enhanced Polymerization Control. *Macromolecules* **2017,** 50, 2696-2705.
28. Zerk, T. J.; Bernhardt, P. V. Solvent dependent anion dissociation limits copper(i) catalysed atom transfer reactions. *Dalton Trans.* **2013,** 42, 11683-11694.
29. Fantin, M.; Lorandi, F.; Gennaro, A.; Isse, A. A.; Matyjaszewski, K. Electron Transfer Reactions in Atom Transfer Radical Polymerization. *Synthesis* **2017,** 49, 3311-3322.
30. Chmielarz, P.; Fantin, M.; Park, S.; Isse, A. A.; Gennaro, A.; Magenau, A. J. D.; Sobkowiak, A.; Matyjaszewski, K. Electrochemically mediated atom transfer radical polymerization (eATRP). *Prog. Polym. Sci.* **2017,** 69, 47-78.
31. Pintauer, T.; Braunecker, W.; Collange, E.; Poli, R.; Matyjaszewski, K. Determination of Rate Constants for the Activation Step in Atom Transfer Radical Polymerization Using the Stopped-Flow Technique. *Macromolecules* **2004,** 37, 2679-2682.
32. Wulkow, M. Computer Aided Modeling of Polymer Reaction Engineering—The Status of Predici, I-Simulation. *Macromol. React. Eng.* **2008,** 2, 461-494.
33. Fischer, H. The Persistent Radical Effect: A Principle for Selective Radical Reactions and Living Radical Polymerizations. *Chem. Rev.* **2001,** 101, 3581-3610.
34. Goldstein, S.; Czapski, G.; Cohen, H.; Meyerstein, D. Formation and decomposition of transient complexes with a copper-carbon .sigma.-bond in the reaction of copper(I) phenanthroline with aliphatic free radicals. A pulse radiolysis study. *Inorg. Chem.* **1988,** 27, 4130-4135.
35. Tang, W.; Kwak, Y.; Braunecker, W.; Tsarevsky, N. V.; Coote, M. L.; Matyjaszewski, K. Understanding Atom Transfer Radical Polymerization: Effect of Ligand and Initiator Structures on the Equilibrium Constants. *J. Am. Chem. Soc.* **2008,** 130, 10702-10713.
36. Lorandi, F.; Fantin, M.; Isse, A. A.; Gennaro, A.; Matyjaszewski, K. New protocol to determine the equilibrium constant of atom transfer radical polymerization. *Electrochim. Acta* **2018,** 260, 648-655.
37. Gorrell, J. H.; Dubois, J. T. Smoluchowski equation for systems which do not obey the Stokes-Einstein relation. *J. Chem. Soc. Faraday Trans.* **1967,** 63, 347-354.
38. Braunecker, W. A.; Tsarevsky, N. V.; Gennaro, A.; Matyjaszewski, K. Thermodynamic Components of the Atom Transfer Radical Polymerization Equilibrium: Quantifying Solvent Effects. *Macromolecules* **2009,** 42, 6348-6360.
39. Ribelli, T. G.; Matyjaszewski, K.; Poli, R. The interaction of carbon-centered radicals with copper(I) and copper(II) complexes. *J. Coord. Chem.* **2018,** 71, 1641-1668.
40. Thevenin, L.; Fliedel, C.; Fantin, M.; Ribelli, T. G.; Matyjaszewski, K.; Poli, R. Reductive Termination of Cyanoisopropyl Radicals by Copper(I) Complexes and Proton Donors: Organometallic Intermediates or Coupled Proton–Electron Transfer? *Inorg. Chem.* **2019**, DOI: 10.1021/acs.inorgchem.9b00660.
41. Shaver, M. P.; Allan, L. E. N.; Gibson, V. C. Organometallic intermediates in the controlled radical polymerization of styrene by α-diimine iron catalysts. *Organometallics* **2007,** 26, 4725-4730.
42. Coward, D. L.; Lake, B. R. M.; Shaver, M. P. Understanding Organometallic-Mediated Radical Polymerization with an Iron(II) Amine-Bis(phenolate). *Organometallics* **2017,** 36, 3322-3328.
43. Kaur, A.; Ribelli, T. G.; Schröder, K.; Matyjaszewski, K.; Pintauer, T. Properties and ATRP Activity of Copper Complexes with Substituted Tris(2-pyridylmethyl)amine-Based Ligands. *Inorg. Chem.* **2015,** 54, 1474-1486.

44. Ribelli, T. G.; Fantin, M.; Daran, J.-C.; Augustine, K. F.; Poli, R.; Matyjaszewski, K. Synthesis and Characterization of the Most Active Copper ATRP Catalyst Based on Tris[(4-dimethylaminopyridyl)methyl]amine. *J. Am. Chem. Soc.* **2018,** 140, 1525-1534.
45. Horn, M.; Matyjaszewski, K. Solvent Effects on the Activation Rate Constant in Atom Transfer Radical Polymerization. *Macromolecules* **2013,** 46, 3350-3357.
46. Krys, P.; Wang, Y.; Matyjaszewski, K.; Harrisson, S. Radical Generation and Termination in SARA ATRP of Methyl Acrylate: Effect of Solvent, Ligand, and Chain Length. *Macromolecules* **2016,** 49, 2977-2984.
47. Jakubowski, W.; Min, K.; Matyjaszewski, K. Activators Regenerated by Electron Transfer for Atom Transfer Radical Polymerization of Styrene. *Macromolecules* **2006,** 39, 39-45.
48. Payne, K. A.; D'hooge, D. R.; Van Steenberge, P. H. M.; Reyniers, M.-F.; Cunningham, M. F.; Hutchinson, R. A.; Marin, G. B. ARGET ATRP of Butyl Methacrylate: Utilizing Kinetic Modeling To Understand Experimental Trends. *Macromolecules* **2013,** 46, 3828-3840.
49. Mohapatra, H.; Kleiman, M.; Esser-Kahn, A. P. Mechanically controlled radical polymerization initiated by ultrasound. *Nat. Chem.* **2016,** 9, 135.

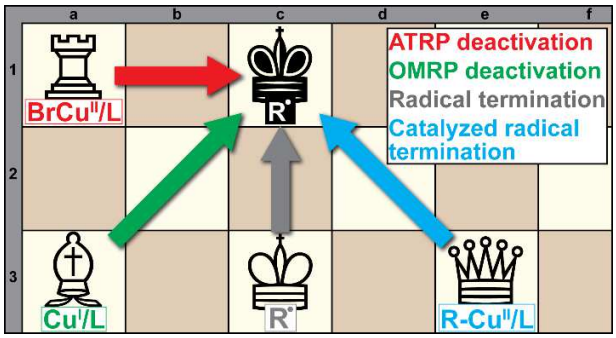

For Table of Contents Only